Percolation thresholds of disks with random nonoverlapping patches on four regular two-dimensional lattices

Jie Wang [1,2] Xuebin Wang,[1] Wenli Liu,[1] and Hao Hu [1,*]

[1]*School of Physics and Optoelectronic Engineering, Anhui University, Hefei, Anhui 230601, China*

[2]*School of Materials Science and Engineering, Anhui University, Hefei, Anhui 230601, China*

(Received 8 February 2024; accepted 13 May 2024; published 3 June 2024)

In percolation of patchy disks on lattices, each site is occupied by a disk, and neighboring disks are regarded as connected when their patches contact. Clusters of connected disks become larger as the patchy coverage of each disk χ increases. At the percolation threshold χ_c, an incipient cluster begins to span the whole lattice. For systems of disks with n symmetric patches on Archimedean lattices, a recent work [Wang *et al.*, Phys. Rev. E **105**, 034118 (2022)] found symmetric properties of $\chi_c(n)$, which are due to the coupling of the patches' symmetry and the lattice geometry. How does χ_c behave with increasing n if the patches are randomly distributed on the disks? We consider two typical random distributions of the patches, i.e., the equilibrium distribution and a distribution from random sequential adsorption. Combining Monte Carlo simulations and the critical polynomial method, we numerically determine χ_c for 106 models of different n on the square, honeycomb, triangular, and kagome lattices. The rules governing $\chi_c(n)$ are investigated in detail. They are quite different from those for disks with symmetric patches and could be useful for understanding similar systems.

DOI: 10.1103/PhysRevE.109.064104

I. INTRODUCTION

The idea of percolation was first applied to the study of polymer gelation by Flory in the 1940's [1]. In the 1950s, Broadbent and Hammersley pioneered the use of percolation as a statistical model [2], and since then percolation has been extensively studied and widely applied [3,4]. Recently percolation theory has been used to understand novel gels [5–7], complex Earth systems [8], epidemiology [9], functional colloids [10], quantum computation [11], etc.

Percolation mainly focuses on the emergence of long-range connectivity. Using site percolation on the square lattice as an example: each lattice site is occupied independently with probability p, and adjacent sites are considered to be connected. When p increases, clusters of connected sites become larger, then an incipient cluster spanning the whole lattice begins to appear at the percolation threshold p_c, i.e., percolation occurs. In different percolation problems, parameters controlling the formation of clusters can be different, but the percolation threshold is always a crucial quantity. There exist rich critical phenomena near the percolation threshold [3,4].

Recently, Wang *et al.* [12] investigated percolation thresholds of disks with symmetrically distributed (SYM-type) patches on two-dimensional (2D) Archimedean lattices. In these models, there is a patchy disk on each lattice site, and two adjacent disks are considered to be connected when their patches cover the same edge. When the proportion of the disk surface covered by patches (denoted as χ) increases, clusters of particles connected by patches become larger, and the system percolates at a threshold χ_c. Reference [12] finds that coupling of the lattice geometry and the patchy symmetry plays an important role in determining χ_c. As a result, when the number of patches on a disk (denoted as n) increases, $\chi_c(n)$ shows a periodic behavior in n. The period n_0 is determined by the lattice geometry, and when $n = n_0$, percolation of patchy disks is equivalent to site percolation on the same lattice. Due to this periodicity, by simulating a finite number of systems, the authors are able to give precise percolation thresholds for systems of disks with an arbitrary number of SYM-type patches on all 11 2D Archimedean lattices [12], which include square, honeycomb, triangular, and kagome lattices.

Surface modification or compartmentalization methods are usually used to design patches in experiments [13–15]. Realizing $n \geqslant 2$ SYM-type patches on disks needs careful operations. If $n \geqslant 2$ patches are randomly distributed on each disk, how does $\chi_c(n)$ change with n? Comparing with systems of disks with SYM-type patches, since there is no explicit coupling between the patchy symmetry and the lattice geometry, the systems will lose the periodicity of $\chi_c(n)$ and the equivalence with site percolation mentioned in the previous paragraph. Would the lattice geometry still affect $\chi_c(n)$, and could the randomness of patches bring new phenomena?

To address the above questions, this paper investigates percolation of disks with random patches on four regular 2D lattices: square, honeycomb, triangular, and kagome. The same as in Ref. [12], we consider that there is a disk at each site of a lattice, and disks are connected when their patches cover the same edge. The patches are randomly distributed on disks instead of being of the SYM type. We assume that there is no overlapping between patches and consider two types of random patches. One is random patches of the equilibrium distribution (EQ type), for which different patchy configurations have the same probability of occurrence. The other

*huhao@ahu.edu.cn

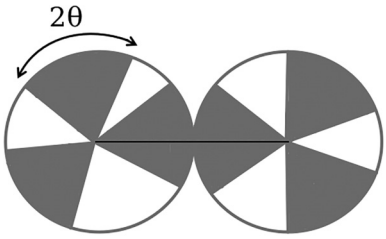

FIG. 1. Illustration of three-patch disks. The gray regions on the disks represent patches of the same size, characterized by the half-patch angle θ. The patches are nonoverlapping, and their positions are random. Adjacent particles are considered connected only when their patches cover the same edge.

is of a nonequilibrium distribution generated by the random sequential adsorption (RSA type) [16].

For systems of disks with the two types of random patches on the four lattices, combining Monte Carlo (MC) simulations and the critical polynomial method [12,17–26], we determine percolation thresholds $\chi_c(n)$ of 106 models in total. We mainly find the following: (i) as n increases, $\chi_c(n)$ approaches the bond percolation threshold p_c on the modified lattice for which a site is added in the middle of each edge of the original lattice. For $n \gtrsim 10$, χ_c deviates from p_c within $O(10^{-3})$. (ii) For $2 < n \lesssim 10$, χ_c^{EQ} is close to but different from χ_c^{RSA}, while they are the same for $n \leqslant 2$. (iii) $\chi_c(n)$ is a nonmonotonic function of n. These results are compared with previous results of χ_c^{SYM}, and understood by observing the coverage of lattice edges by patches on a single disk. The results can provide useful references for further studies on phase transitions and critical phenomena in similar systems [10,12,27–32].

The remaining parts of this paper are arranged as follows. Section II introduces the models and methods. Section III presents our main results. A brief conclusion and discussion is given in Sec. IV.

II. MODELS AND METHODS

A. Models

We study percolation thresholds of model systems of disks with randomly placed patches on four lattices: square, honeycomb, triangular, and kagome. Periodic boundary conditions are applied. The boundary shape of the square lattice is chosen as square, and those of the other three lattices are chosen as rhombus. Each lattice site is occupied by a disk-shaped particle, with the center of the disk located at the site. The diameters of all disks are the same and equal to the distance between nearest-neighboring lattice sites. Every disk is randomly decorated with n nonoverlapping patches of the same size. The size of a patch is θ, defined as half of the angle occupied by the patch. Adjacent disks are considered to be connected only when their patches cover the same edge of the lattice, i.e., the patches contact. For example, Fig. 1 illustrates two connected three-patch disks. When changing θ, all patches' positions are taken at random again. As θ increases, clusters of disks connected by patches grow larger on the lattice. At the percolation threshold θ_c, a cluster spanning the whole lattice appears with a finite probability for the first time. Figure 2 exemplifies the percolation of two-patch disks on the square lattice. For the comparison of percolation thresholds of systems with different n, we use the surface coverage χ to represent the controlling parameter, which is given by

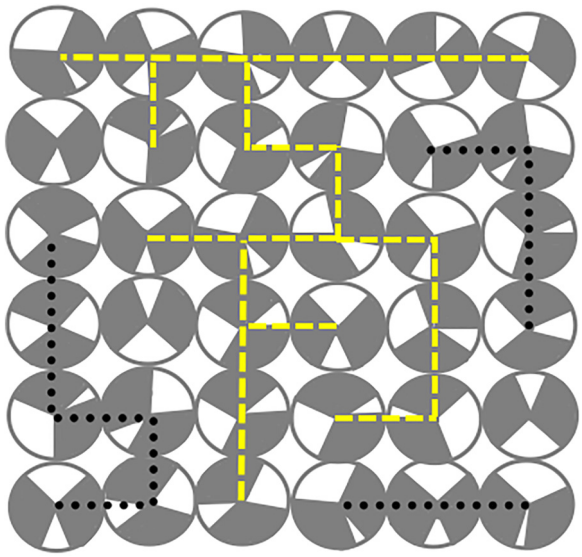

FIG. 2. Snapshot for percolation of two-patch disks on the square lattice. The spanning cluster is labeled by connected dashed lines.

$$\chi = 2n\theta/2\pi = n\theta/\pi. \tag{1}$$

Using MC methods, we simulated models on the square lattice with $2 \leqslant n \leqslant 14$, the honeycomb lattice with $2 \leqslant n \leqslant 13$, the triangular lattice with $2 \leqslant n \leqslant 18$, and the kagome lattice with $2 \leqslant n \leqslant 12$. On the four lattices with linear size L, the total number of disks are L^2, $L^2/2$, L^2, and $3L^2/4$, respectively [12]. We conducted simulations at different χ and three sizes $L = 16$, 32, 64. For each pair of (χ, L), at least 10^6 independent configurations were generated. We combined the simulation results with the critical polynomial method to estimate χ_c [12,26]. The methods for determining χ_c and for placing random nonoverlapping patches in MC simulations are described in the next two subsections, respectively.

B. Critical polynomial method for determining percolation thresholds

The critical polynomial method is an effective approach for calculating 2D percolation thresholds. For a 2D lattice B with periodic boundary conditions, the probabilistic geometric definition of the critical polynomial is given by [21]

$$P_B \equiv R_2 - R_0. \tag{2}$$

Here R represents the wrapping probability [33,34]. When mapping B onto the torus, for a configuration of the percolation model, we say that it is wrapping if there exists a cluster satisfying the following. Starting from a point on the cluster, a walker can follow the cluster, cross the boundary, and return to the starting point. R_2 represents the probability of wrapping in two directions, and R_0 represents the probability of no wrapping. In principle P_B can be expressed as polynomials of the occupation probability p or the surface coverage χ on finite lattices.

Due to the universality of critical behaviors [21], the solution for $P_B = 0$ provides an estimate of the percolation threshold. For models with exact solutions of the percolation threshold, the smallest B can provide the exact threshold value. For models without available exact solutions, it has been found that the root of $P_B = 0$ converges to the threshold very rapidly as the size of B increases [12,25,26]. For example, for the bond percolation on a $L \times \infty$ kagome lattice with bond occupation probability p, the root $p(L)$ of $P_B(p, L) = 0$ for $L \leqslant 16$ was obtained to high precision in Ref. [25]. It was found that $p_c(L) \simeq p_c + A_1/L^6$, where A_1 is a nonuniversal amplitude. The precision of p_c on the kagome lattice, as provided in Ref. [25], reaches up to the 17th decimal place, far exceeding results obtained through MC methods. On 2D Archimedean lattices, for disks with SYM-type patches, Ref. [12] employed MC simulations to compute P_B near χ_c, and obtained precise estimations of χ_c by fitting the data to the finite-size scaling formula [12,26]:

$$P_B(\chi, L) \simeq a_1(\chi - \chi_c)L^{y_t} + b_1 L^{y_1}. \tag{3}$$

Here $y_t = 1/\nu = 3/4$ represents the thermal renormalization exponent, $y_1 < 0$ is the leading irrelevant exponent, and a_1 and b_1 are nonuniversal amplitudes. For systems of patchy disks in Ref. [12], it is found that $y_1 \lesssim -3$. By setting $P_B(\chi, L) = 0$ from Eq. (3), we obtain $\chi(L) \simeq \chi_c - (b_1/a_1)L^{y_1 - y_t}$, which implies that the root of $P_B = 0$ approaches χ_c with a rate of $L^{-3.75}$ or faster. Such small finite-size corrections allow for obtaining estimates of χ_c with high precision without simulating systems of large L. Reference [12] has numerically estimated χ_c for 88 systems of particles with SYM-type patches, with an accuracy to the sixth decimal place or even higher. In this paper, for disks with random patches, we also calculate P_B by MC simulations and estimate χ_c by fitting the data to Eq. (3).

C. Monte Carlo methods for randomly placing patches

For $n = 1$, the disks are randomly oriented, and there is no difference between the SYM-type patches and random patches. When $n \geqslant 2$, random nonoverlapping patches on the particle surface can follow different distributions. We consider two typical distributions: one is the EQ type, for which patches on a particles are in equilibrium and different patchy configurations occur with an equal probability; the other is the RSA type, for which patches are placed by random sequential adsorption [16] and probabilities of different patchy configurations can be different. Below we present details for realizing these two types of random nonoverlapping patches in MC simulations.

For EQ-type patches, when n is small, we simultaneously generate n random numbers to give positions of all patches. If there is overlapping of patches, we regenerate n random numbers until nonoverlapping patches are obtained. When n is large, since the efficiency of the above procedure is low, we employ the following method of random rotations: placing n patches symmetrically on the disk, then attempting random rotations of the patches one by one (this sequential updating is faster than randomly selecting a patch to rotate [35], and the balance condition is satisfied for the convergence to equilibrium [36]). After a sufficient number of rotations, the patches reach the equilibrium distribution with randomized positions. Figure 3(a) illustrates the above rotation method of realizing the EQ-type patches. The rotation amplitude is chosen as $(1 - \chi)/n$, i.e., each time a patch center is proposed to rotate by a uniformly random angle in $2\pi[-(1 - \chi)/n, (1 - \chi)/n]$. This choice is close to $2.5(1 - \chi)/n$ used in Ref. [35]. Test simulations are performed to identify the appropriate number of rotations. In the tests we observe the coverage of neighboring edges by the patches of a disk. Defining one sweep as an attempt to rotate each patch once, we set a small number of sweeps m_s and a larger number of sweeps m_s'. If occurrence probabilities of coverage structures obtained from m_s sweeps and those from m_s' sweeps are consistent within $O(10^{-4})$, we use m_s in formal simulations. For example, Table I provides occurrence probabilities $p(z)$ of local structures with z edges being covered by patches of a disk, for the model of $n = 7$ on the square lattice at $\chi = 0.7084$, with $m_s = 60$ and $m_s' = 300$. Figure 4 shows that P_B values obtained from these two numbers of sweeps are consistent at $L = 16$, 32, and 64. This confirms the reliability of the estimated χ_c from $m_s = 60$. To obtain EQ-type patches, we used the above method of random rotations for $n > 6$, 5, 10, 5 on the square, honeycomb, triangular, and kagome lattices, respectively.

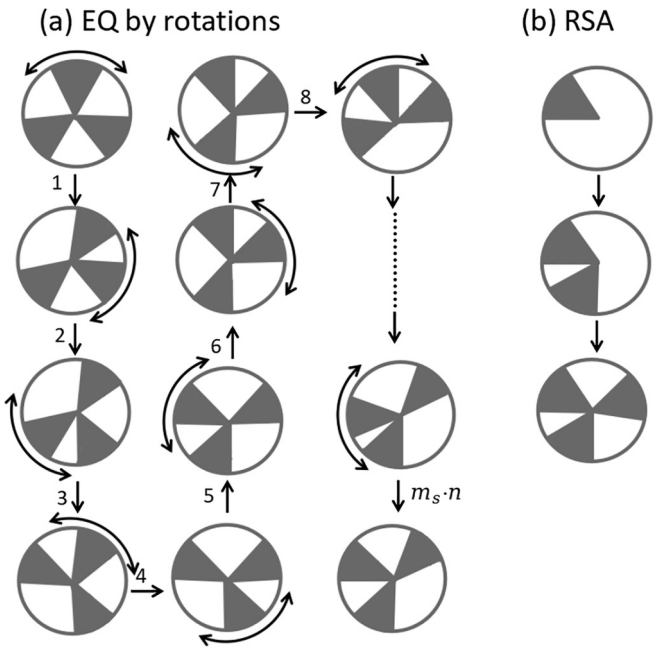

FIG. 3. Procedures for generating $n = 3$ random nonoverlapping patches on a disk. (a) EQ-type patches can be realized by $m_s n$ trial random rotations, in which n rotations make a sweep and m_s is the number of sweeps. A double-arrow curve represents the rotation range for the center of a patch. Sequential rotations of patches are attempted. A rotation is rejected if it leads to overlapping of patches. (b) For the RSA type, patches are sequentially placed in the available space of a disk.

For RSA-type patches, placing n patches is equivalent to the RSA of n nonoverlapping line segments of length χ/n, in one-dimensional (1D) continuous space of unit length, with the periodic boundary condition [16]. We employ the following MC method [37] to obtain the RSA-type patches:

TABLE I. Simulation results for disks with $n = 7$ EQ-type patches on the square lattice at $\chi = 0.7084$. The quantity $p(z)$ is the occurrence probability of local structures with z edges being covered by patches of a particle. The parameters m_s and m_s' denote the number of sweeps used for obtaining EQ-type patches through random rotations.

	$m_s = 60$	$m_s' = 300$
$p(0)$	0.00710(4)	0.00711(4)
$p(1)$	0.0626(1)	0.0628(1)
$p(2)$	0.2366(2)	0.2367(2)
$p(3)$	0.4770(2)	0.4769(2)
$p(4)$	0.2166(2)	0.2164(2)

(i) Generate a uniformly distributed random number within the range [0,1) to determine the position of the first patch. Compute the length l of the available space where the next patch can be placed. (ii) If the number of placed patches is smaller than n and $l = 0$, clear the existing patches and return to step (i). Otherwise, generate a uniformly random number within the range $[0, l)$ to randomly place a patch in the available space, which consists of one or more continuous regions where a patch can still be placed. Placing the patch separates a continuous region into two continuous regions. For each of the two regions, check whether a patch can be contained, and if it is possible, record the information of the region and update the length l. (iii) Repeat step (ii) until n patches are all placed. Figure 3(b) illustrates the RSA process.

III. RESULTS

In this section we present percolation thresholds χ_c for disks with two types of random patches on four lattices. The variations of χ_c with the number of patches n are investigated in detail.

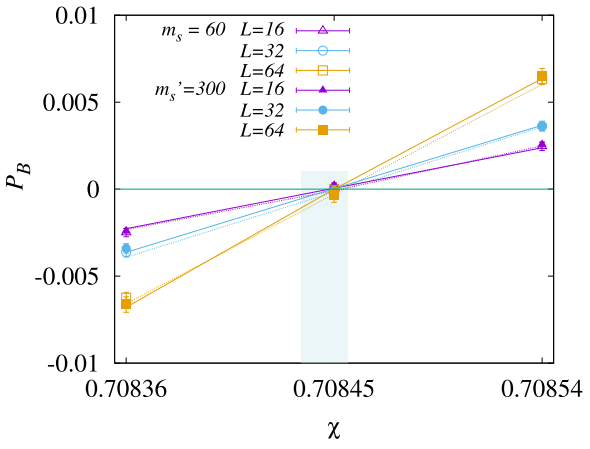

FIG. 4. The quantity P_B vs χ for the system of disks with $n = 7$ EQ-type patches on the square lattice. Results obtained by using $m_s = 60$ and $m_s' = 300$ are consistent with each other. Fitting the data to Eq. (3) yields $\chi_c(m_s = 60) = 0.708\,444(4)$ and $\chi_c(m_s' = 300) = 0.708\,448(8)$. The light shaded region represents the combined estimate $\chi_c = 0.708\,446(10)$ from the above two results. The lines correspond to fits with Eq. (3).

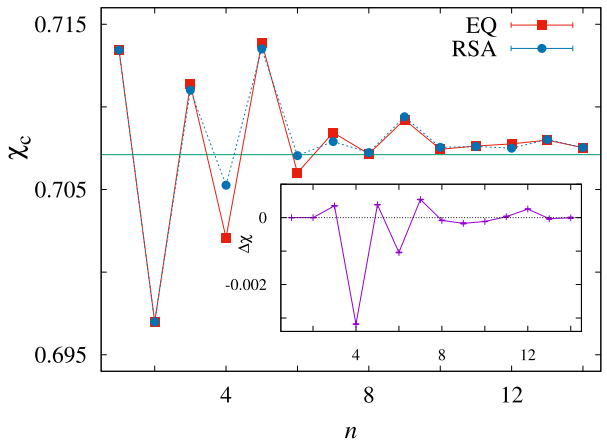

FIG. 5. Percolation threshold χ_c vs the number of patches n on the square lattice, for systems of disks with EQ-type and RSA-type patches. The horizontal straight line represents the bond percolation threshold $p_c = 1/\sqrt{2} \simeq 0.7071$ for the modified square lattice, for which a site is added at the middle of each edge of the original square lattice. The inset shows $\Delta\chi = \chi_c^{\mathrm{EQ}} - \chi_c^{\mathrm{RSA}}$ vs n. Error bars are smaller than the data points.

A. Results on the square lattice

On the square lattice, it was found that, for disks with SYM-type patches, thresholds $\chi_c(n)$ repeat in a period of 4 when increasing n [12]. When patches are randomly placed, we numerically determined $\chi_c(n)$ for $n \leqslant 14$ as shown in Table II and plotted in Fig. 5. Snapshots of random patchy configurations near $\chi_c(n)$ are shown in Fig. 6. Observing these values of $\chi_c(n)$, we find three rules: (i) As n increases, χ_c approaches the bond percolation $p_c = 1/\sqrt{2} \simeq 0.7071$ on a modified square lattice (for which a site is added in the middle of each edge of the original square lattice). (ii) For $n > 2$, χ_c^{EQ} and χ_c^{RSA} are close but different. (iii) $\chi_c(n)$ is a nonmonotonic function of n, having local minimum values at even n when n is small. These three rules are explored as follows.

For understanding the first rule, we treat the circumference of a disk as a 1D system with the periodic boundary condition. In the 1D system, random patches on a disk are regarded as particles with hardcore interactions, and the lattice edges associated with the center of the disk are considered as equally separated fixed positions. When fixing χ, as $n \to \infty$, the size of particles in the 1D system tends to zero, and the distance between neighboring edges is much larger than the particle size. Thus, the occupation of different edges by patches is uncorrelated, regardless of whether the patches are of the EQ type [38,39] or the RSA type [16]. Moreover, for any given lattice edge, since the orientation of a disk is random, the probability of the edge being covered by patches of the disk is χ. These lead to that, in the limit $n \to \infty$, percolation of disks with random nonoverlapping patches on the square lattice is equivalent to standard bond percolation on the modified square lattice, for which a site is added at the middle of each edge of the original square lattice. Since bond percolation threshold on the square lattice is $p_c = 1/2$, $\chi_c(n \to \infty)$ satisfies $\chi_c^2 = p_c$, i.e., $\chi_c(n \to \infty) = 1/\sqrt{2}$. From Table II, for $10 \leqslant n \leqslant 14$, the relative error between $\chi_c(n)$ and $\chi_c(n \to \infty)$ is of the order $O(10^{-4})$.

TABLE II. Percolation threshold χ_c for systems of $n \leqslant 14$ on the square lattice. A system consists of disks with n random patches of the EQ type or RSA type. For comparison, we also include $\chi_c^{\rm SYM}$ for systems of disks with n symmetrically placed patches, which are from Ref. [12]. The latter exhibits a periodicity of 4, i.e., $\chi_c^{\rm SYM}(n) = \chi_c^{\rm SYM}(\mathrm{mod}(n, 4))$.

n	1	2	3	4
$\chi_c^{\rm SYM}$	0.713 444 50(3)	0.676 345 5(3)	0.713 444 6(3)	0.592 746 5(4)
$\chi_c^{\rm EQ}$		0.696 989 (2)	0.711 370 (2)	0.702 079 (6)
$\chi_c^{\rm RSA}$		0.696 989 (4)	0.711 017 (4)	0.705 262 (8)
n	5	6	7	8
$\chi_c^{\rm EQ}$	0.713 897 (6)	0.706 01 (1)	0.708 444 (4)	0.707 15 (1)
$\chi_c^{\rm RSA}$	0.713 509 (6)	0.707 051 (6)	0.707 903 (3)	0.707 231 (4)
n	9	10	11	12
$\chi_c^{\rm EQ}$	0.709 230 (6)	0.707 437 (6)	0.707 63 (2)	0.707 759 (8)
$\chi_c^{\rm RSA}$	0.709 40 (2)	0.707 55 (2)	0.707 606 (3)	0.707 502 (2)
n	13	14		
$\chi_c^{\rm EQ}$	0.707 99 (2)	0.707 532 (8)		
$\chi_c^{\rm RSA}$	0.708 02 (1)	0.707 536 (3)		

Considering the second rule, the difference between $\chi_c^{\rm EQ}$ and $\chi_c^{\rm RSA}$ is due to that patches of EQ type and of RSA type follow difference distributions when $n > 2$. Patches of the EQ type follow an equilibrium distribution, for which different patchy configurations of a disk appear with the same probability, while patches of the RSA type follow a nonequilibrium distribution, for which probabilities of different patchy configurations can be different [16]. In Appendix A we illustrate the above difference by considering the occupation of three edges by three patches of a disk. For $n = 2$, as explained in Appendix B, the difference between the two types of random patches disappears, thus $\chi_c^{\rm EQ}(2) = \chi_c^{\rm RSA}(2)$.

Finally, for the third rule, we find that for both types of random patches, $\chi_c(n)$ exhibits local minimum values at even n for $n < 12$. The occurrence of local minima can be understood by looking at the probability $p(n, z)$ for a particle with n patches covering z neighboring edges. In Fig. 12 in Appendix C, we plot $p(n, z)$ at $\chi_c(n)$ for systems with $1 \leqslant n \leqslant 5$ RSA-type patches. It can be observed that $p(n, z = 4)$ has local maxima at $n = 2$ and 4, accompanied by local minima of $p(n, z = 3)$ at same n values. The local minima of $\chi_c(n)$ are correlated with the appearance of these local extrema of $p(n, z)$. Similar results are obtained for systems of disks with EQ-type patches. The considerable large difference of $|\Delta\chi|$ at $n = 4$ in Fig. 5 is related to that on average EQ-type patches appear more uniform than RSA-type patches, which leads to larger $p(4, 4)$.

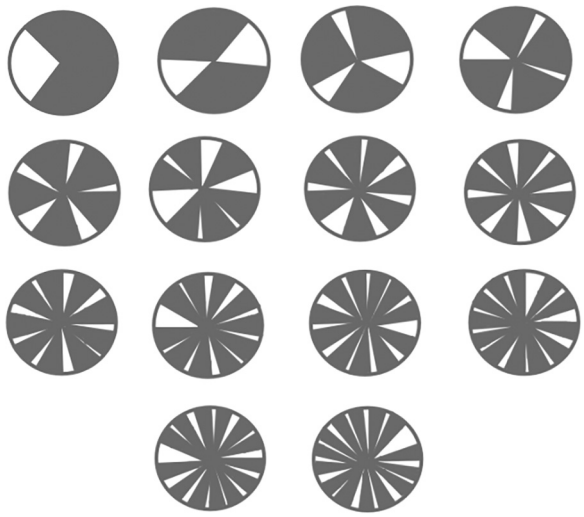

FIG. 6. Snapshots of random patchy configurations near $\chi_c(n)$ of the square lattice models, with $n = 1$ to 14.

B. Results on honeycomb, triangular, and kagome lattices

We also observe the variation of χ_c with n on the honeycomb, triangular, and kagome lattices, The results are described below.

On the honeycomb lattice, for disks with SYM-type patches, it was found that $\chi_c(n)$ shows a period of 3 as n increases [12]. When patches are of the EQ type or RSA type, we numerically determined χ_c for systems with $n \leqslant 13$, which are summarized in Table III and plotted in Fig. 7. Observing these results, we find the following four rules. (i) As n increases, $\chi_c(n)$ approaches the bond percolation threshold of a modified honeycomb lattice (for which a site is added in the middle of each edge of the honeycomb lattice), i.e., $\chi_c(n \to \infty) = \sqrt{1 - 2\sin(\pi/18)} \simeq 0.8079$, where $1 - 2\sin(\pi/18)$ [40] is the bond percolation threshold of the original honeycomb lattice. (ii) When $n > 2$, it is found that $\chi_c^{\rm EQ}$ and $\chi_c^{\rm RSA}$ are close but different. The above rules (i) and (ii) are similar to those on the square lattice, and they can be understood in the same ways as in Sec. III A. (iii) $\chi_c(n)$ is a nonmonotonic function of n and exhibits local minima when $\mathrm{mod}(n, 3) = 0$ for $n \leqslant 13$. Similar to that on the square lattice, this observation can be explained by calculating the probability $p(n, z)$ of a disk with n patches covering z neighboring edges at $\chi_c(n)$. Figure 13 in Appendix C shows $p(n, z)$ for systems of disks with RSA-type patches on the honeycomb lattice. It can be seen that $p(n, 3)$ has local maxima at $n = 3$ and 6, which is correlated with the appearance of local minima of $\chi_c(n)$ at $n = 3$ and 6, respectively. Similar results of $p(n, z)$

TABLE III. Percolation threshold χ_c for systems of $n \leqslant 13$ on the honeycomb lattice. A system consists of disks with n random patches of the EQ type or RSA type. For comparison, we also include $\chi_c^{\rm SYM}$ for systems of disks with n symmetrically placed patches, which are from Ref. [12]. The latter exhibits a periodicity of 3, i.e., $\chi_c^{\rm SYM}(n) = \chi_c^{\rm SYM}(\mathrm{mod}(n, 3))$.

n	1	2	3	4	5
$\chi_c^{\rm SYM}$	0.815 301 86(3)	0.815 301 6(3)	0.697 040 4(9)		
$\chi_c^{\rm EQ}$		0.815 301 (4)	0.789 621 (2)	0.813 03 (1)	0.814 889(8)
$\chi_c^{\rm RSA}$		0.815 301 (4)	0.794 664 (4)	0.812 089(2)	0.814 719 (2)
n	6	7	8	9	10
$\chi_c^{\rm EQ}$	0.799 15 (2)	0.811 56 (1)	0.811 960 (4)	0.802 940 (4)	0.811 129 (4)
$\chi_c^{\rm RSA}$	0.803 878 (8)	0.811 118(3)	0.810 78 (1)	0.805 575 (4)	0.810 784(4)
n	11	12	13		
$\chi_c^{\rm EQ}$	0.810 162 (4)	0.804 976 (5)	0.810 483(8)		
$\chi_c^{\rm RSA}$	0.809 463 (6)	0.806 929 (9)	0.809 782(4)		

are obtained for systems of disks with EQ-type patches. The considerable large difference of $|\Delta\chi|$ at $\mod(n, 3) = 0$ in Fig. 7 is related to that on average EQ-type patches appear more uniform than RSA-type patches, which leads to larger $p(n, 3)$. (iv) When $n = 2$, it is found that $\chi_c^{\rm EQ} = \chi_c^{\rm RSA} = \chi_c^{\rm SYM}$. This is different from results on the square lattice, where $\chi_c^{\rm SYM}$ is different from $\chi_c^{\rm EQ} = \chi_c^{\rm RSA}$. In Ref. [12], it is shown that for disks with SYM-type patches $\chi_c(1) = \chi_c(2)$. Considering the above and that $\chi_c(1)$ is independent of the types of patches, we conclude that on the honeycomb lattice $\chi_c(1) = \chi_c(2)$, for all three types of patches. In Appendix D we provide a detailed explanation of rule (iv) by calculating probabilities of a disk with its patches covering different numbers of edges.

On the triangular lattice, for disks with SYM-type patches, it was found that $\chi_c(n)$ shows a period of 6 as n increases [12]. When patches are of the EQ type or RSA type, we numerically

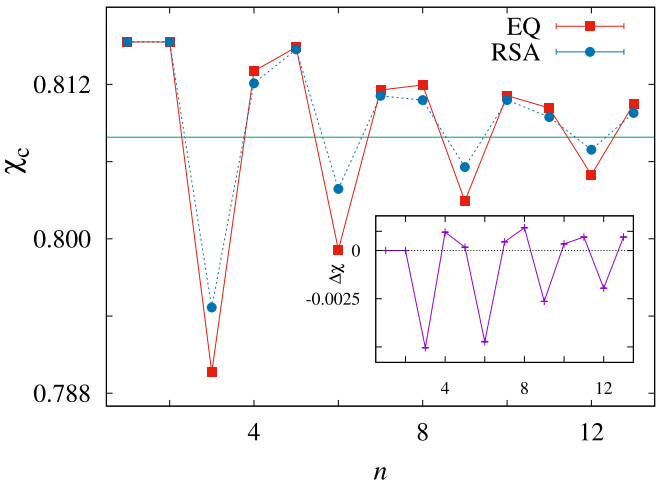

FIG. 7. Percolation threshold χ_c vs the number of patches n on the honeycomb lattice, for systems of disks with EQ-type and RSA-type patches. The horizontal straight line represents the bond percolation threshold $p_c = \sqrt{1 - 2\sin(\pi/18)} \simeq 0.8079$ for the modified honeycomb lattice, for which a site is added at the middle of each edge of the original honeycomb lattice. The inset shows $\Delta\chi = \chi_c^{\rm EQ} - \chi_c^{\rm RSA}$ vs n. Error bars are smaller than the data points.

determined χ_c for systems with $n \leqslant 18$, which are summarized in Table IV and plotted in Fig. 8. Observing these results, we find the following three rules. (i) As n increases, $\chi_c(n)$ approaches the bond percolation threshold of a modified triangular lattice (for which a site is added in the middle of each edge of the triangular lattice), i.e., $\chi_c(n \to \infty) = \sqrt{2\sin(\pi/18)} \simeq 0.5893$, where $2\sin(\pi/18)$ [40] is the bond percolation threshold of the triangular lattice. (ii) When $n > 2$, it is found that $\chi_c^{\rm EQ}$ and $\chi_c^{\rm RSA}$ are close but different. Rules (i) and (ii) are similar to those on the square lattice, and they can be understood in same ways as in Sec. III A. (iii) $\chi_c(n)$ is a nonmonotonic function of n, and exhibits a minimum at $n = 3$. This can be explained by calculating the probability $p(n, z)$ of a particle with n patches covering z neighboring edges at $\chi_c(n)$. Figure 14 in Appendix C shows $p(n, z)$ for systems of disks with RSA-type patches on the triangular lattice. It can be seen that both $p(n, 5)$ and $p(n, 3)$ have a maximum at $n = 3$, which is correlated with the appearance of the minimum of $\chi_c(n)$ at $n = 3$. Comparing with the square and honeycomb lattices, here the positions of minima (given by specific values of n) do not appear periodically for small n values, which should be due to that a site is connected to more edges on the triangular lattice. Similar results are obtained for systems of disks with EQ-type patches.

On the kagome lattice, for disks with SYM-type patches, it was found that $\chi_c(n)$ shows a period of 6 as n increases [12]. When patches are of the EQ-type or RSA-type, we numerically determined χ_c for systems with $n \leqslant 12$, which are summarized in Table V and plotted in Fig. 9. Observing these results, we find the following three rules. (i) As n increases, $\chi_c(n)$ approaches the bond percolation threshold of a modified kagome lattice (for which a site is added in the middle of each edge of the kagome lattice), i.e., $\chi_c(n \to \infty) = \sqrt{p_c} \simeq 0.7242$, where $p_c = 0.524\,404\,999\,167\,448\,20(1)$ [25] is the bond percolation threshold of the kagome lattice. (ii) When $n > 2$, it is found that $\chi_c^{\rm EQ}$ and $\chi_c^{\rm RSA}$ are close but different. Rules (i) and (ii) are also similar to those on the square lattice, and they can also be understood in the same ways as in Sec. III A. (iii) $\chi_c(n)$ is a nonmonotonic function of n, and exhibits local minima at even n when $n < 6$. This can also be explained by calculating the probability $p(n, z)$ of a particle with n patches covering z neighboring edges at $\chi_c(n)$.

TABLE IV. Percolation threshold χ_c for systems of $n \leqslant 18$ on the triangular lattice. A system consists of disks with n random patches of the EQ type or RSA type. For comparison, we also include χ_c^{SYM} for systems of disks with n symmetrically placed patches, which are from Ref. [12]. The latter exhibits a periodicity of 6, i.e., $\chi_c^{\mathrm{SYM}}(n) = \chi_c^{\mathrm{SYM}}(\mathrm{mod}(n, 6))$.

n	1	2	3	4	5	6
χ_c^{SYM}	0.627 765 41(3)	0.554 469 9(4)	0.558 806 6(7)	0.554 469 2(4)	0.627 765 6(4)	0.500 000 1(5)
χ_c^{EQ}		0.587 793 (6)	0.575 869 (4)	0.582 391(10)	0.592 885 (6)	0.595 297 (8)
χ_c^{RSA}		0.587 793 (2)	0.575 214 (2)	0.580 971(2)	0.593 240 (6)	0.596 424 (8)
n	7	8	9	10	11	12
χ_c^{EQ}	0.590 80 (2)	0.587 039 (6)	0.588 44 (1)	0.590 24 (2)	0.590 42 (2)	0.589 485 (6)
χ_c^{RSA}	0.593 81 (1)	0.588 096 (10)	0.587 65 (2)	0.588 922 (5)	0.589 931 (6)	0.589 00 (1)
n	13	14	15	16	17	18
χ_c^{EQ}	0.589 081 (8)	0.589 32 (2)	0.589 60 (2)	0.589 62 (1)	0.589 44 (2)	0.589 40 (2)
χ_c^{RSA}	0.589 698 (6)	0.589 399 (6)	0.589 35 (2)	0.589 421 (8)	0.589 494 (8)	0.589 50 (1)

Figure 15 in Appendix C shows $p(n, z)$ for systems of disks with RSA-type patches on the kagome lattice. It can be seen that $p(n, 2)$ and $p(n, 4)$ have local maxima at $n = 2$ and 4. These maxima are correlated with the appearance of local minima of $\chi_c(n)$ at $n = 2$ and 4. Similar results are obtained for systems of disks with EQ-type patches.

IV. CONCLUSION AND DISCUSSION

We have studied percolation thresholds $\chi_c(n)$ for disks with n random nonoverlapping patches on lattices. We consider two types of random patches, EQ type and RSA type, and four regular lattices, square, honeycomb, triangular, and kagome lattices. By combining MC simulations and the critical polynomial method, we accurately estimate χ_c of 106 models, then observe the change of $\chi_c(n)$. We mainly find the following rules. (i) As n increases, $\chi_c(n)$ approaches the bond percolation threshold of the modified lattice, for which a site is added in the middle of each edge of the original lattice. This originates from that, when $n \to \infty$, the patches near different edges are uncorrelated, and that an edge is covered by patches with probability χ. For the largest n values simulated (12 to 18), $\chi_c(n)$ values deviate from the bond percolation threshold by around 10^{-4} to 10^{-3}. It is found in Ref. [12] that, for disks with SYM-type patches, when the symmetry of patches matches that of the lattice, the percolation of patchy disks is equivalent to site percolation. The relation to bond percolation found in this work strengthens the connection between percolation of patchy particles and standard percolation models. (ii) When $n = 2$, $\chi_c^{\mathrm{EQ}} = \chi_c^{\mathrm{RSA}}$; however, when $n > 2$, χ_c^{EQ} and χ_c^{RSA} are close but different. The latter difference is due to that patches of EQ type and RSA type have different distribution when $n > 2$. (iii) $\chi_c(n)$ is a nonmonotonic function of n, especially when n is small. For example, on the square lattice $\chi_c(n)$ has local minima at even n when $n < 12$, and on the honeycomb lattice χ_c shows local minima when n is a multiple of 3 for $n < 13$. In Ref. [12] the authors find that $\chi_c(1)$ is mainly affected by the lattice geometry, but that for systems of particles with $n \geqslant 2$ SYM-type patches, the coupling of patchy symmetry and lattice geometry leads to nonmonotonic changes in $\chi_c(n)$. For systems of $n \geqslant 2$ random nonoverlapping patches, our results show that distributions of patches still couple with the lattice geometry to yield the nonmonotonic behavior of $\chi_c(n)$. We expect that the above results can be generalized to other 2D lattices.

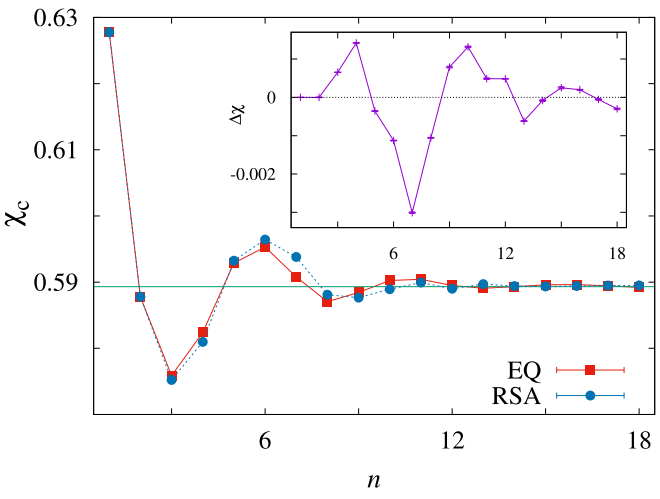

FIG. 8. Percolation threshold χ_c vs the number of patches n on the triangular lattice, for systems of disks with EQ-type and RSA-type patches. The horizontal straight line represents the bond percolation threshold $p_c = \sqrt{2\sin(\pi/18)} \simeq 0.5893$ for the modified triangular lattice, for which a site is added at the middle of each edge of the original triangular lattice. The inset shows $\Delta\chi = \chi_c^{\mathrm{EQ}} - \chi_c^{\mathrm{RSA}}$ vs n. Error bars are smaller than the data points.

If the patchy disks are put in continuous space instead of lattices, how does χ_c change with n? For saturated random sequential adsorbed nonoverlapping disks in 2D continuous space, our preliminary results [41] show that χ_c still shows a nonmonotonic variation with n, regardless of whether patches on the disk are distributed symmetrically or randomly. It is also found that, as $n \to \infty$, percolation of disks with random patches is equivalent to a bond percolation model [41]. The latter can be explained in the same way as on the lattices. The nonmonotonic behavior of χ_c may due to that, in the continuous space, the distribution of neighbors of a disk has certain structural features, which lead to smaller χ_c values when n matches them. We leave a detailed study in the continuous space for future work.

TABLE V. Percolation threshold χ_c for systems of $n \leqslant 12$ on the kagome lattice. A system consists of disks with n random patches of the EQ type or RSA type. For comparison, we also include $\chi_c^{\rm SYM}$ for systems of disks with n symmetrically placed patches, which are from Ref. [12]. The latter exhibits a periodicity of 6, i.e., $\chi_c^{\rm SYM}(n) = \chi_c^{\rm SYM}(\mathrm{mod}(n, 6))$.

n	1	2	3	4	5	6
$\chi_c^{\rm SYM}$	0.745 229 66(5)	0.687 495 0(2)	0.725 743 3(6)	0.687 494 9(4)	0.745 229 4(8)	0.652 701 (2)
$\chi_c^{\rm EQ}$		0.718 116 (2)	0.720 482 (6)	0.709 937 (6)	0.731 606 (8)	0.729 44 (1)
$\chi_c^{\rm RSA}$		0.718 116 (4)	0.722 158 (10)	0.711 080 (8)	0.729 077 (8)	0.731 672 (10)
n	7	8	9	10	11	12
$\chi_c^{\rm EQ}$	0.735 00 (2)	0.722 09 (2)	0.718 74 (2)	0.722 209 (5)	0.726 966 (8)	0.727 61 (2)
$\chi_c^{\rm RSA}$	0.736 08 (2)	0.725 13 (1)	0.719 895 (6)	0.720 92 (2)	0.724 59 (2)	0.726 03 (2)

Finally, it is noted that, both in this work and in Ref. [12], the phenomena are understood by observing the probability $p(n, z)$ of a disk with n patches covering z neighboring edges. Similar observations have been made in Ref. [42] in understanding the relationship between the susceptible-infected-recovered model and standard percolation. In Ref. [12] it is already found that, for fixed n and z, $p(n, z)$ can still be decomposed into probabilities of different local structures whose variations may affect χ_c. It is worth exploring further to find useful formula for predicting χ_c values for systems of patchy particles. It is also noted that there are studies on percolation models of restricted valencies on lattices, such as Ref. [43]. Controlling the numbers, sizes, and positions of patches on particles is a natural way to tune the valencies.

ACKNOWLEDGMENTS

This work has been supported by the National Natural Science Foundation of China under grant No. 12375026 and No. 11905001. We acknowledge the High-Performance Computing Platform of Anhui University for providing computing resources.

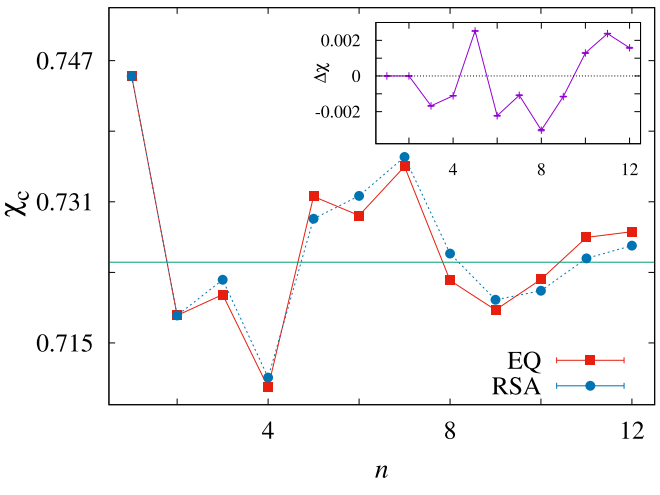

FIG. 9. Percolation threshold χ_c vs the number of patches n on the kagome lattice, for systems of disks with EQ-type and RSA-type patches. The horizontal straight line represents the bond percolation threshold $p_c \simeq 0.7242$ for the modified kagome lattice, for which a site is added at the middle of each edge of the original kagome lattice. The inset shows $\Delta\chi = \chi_c^{\rm EQ} - \chi_c^{\rm RSA}$ vs n. Error bars are smaller than the data points.

APPENDIX A: OCCUPATION OF THREE EDGES BY THREE RANDOM NONOVERLAPPING PATCHES

We take the occupation of three edges by three patches as an example to illustrate that EQ-type and RSA-type random patches lead to different occupation probabilities. As in Fig. 10(a), three edges divide a disk area into three equal regions. For convenience of the analysis below, we assume that the size of a patch satisfies $\alpha = 2\theta < 2\pi/3$ and $4\alpha = 8\theta > 2\pi$. The first inequality says that a patch can occupy at most one edge. The second inequality ensures that at most one patch can be placed within one region, and that in realizing the RSA-type patches the available space always consists of one continuous region.

For patches of the EQ-type, three random numbers in $[0, 2\pi)$ are used to give positions to the three patches. The probability that the three patches do not overlap is

$$\frac{Z(n=3)}{Z} = \frac{2\pi}{2\pi}\left(\int_0^{2\pi-3\alpha} \frac{d\varphi}{2\pi}\frac{2\pi-3\alpha-\varphi}{2\pi} + \int_\alpha^{2\pi-2\alpha} \frac{d\varphi}{2\pi}\frac{\varphi-\alpha}{2\pi}\right) = \frac{(2\pi-3\alpha)^2}{4\pi^2}, \quad \text{(A1)}$$

where definitions of parameters α, φ, and ω are given in Fig. 10(b). The probability that the three patches do not over-

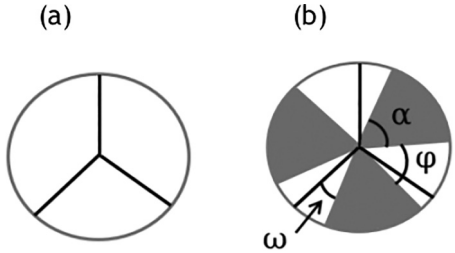

FIG. 10. (a) Three lattice edges divide a disk into three regions of equal area. (b) A configuration in which three patches are randomly placed on a disk and they occupy no edge.

lap and do not occupy any edge is

$$\frac{Z(n=3,z=0)}{Z} = 3\int_0^{\frac{2\pi}{3}-\alpha}\frac{d\omega}{2\pi}\left(\int_{\frac{2\pi}{3}-\omega-\alpha}^{\frac{2\cdot(2\pi)}{3}-\omega-2\alpha}\frac{d\varphi}{2\pi}\frac{\frac{2\pi}{3}-\alpha}{2\pi} + \int_{\frac{2\cdot(2\pi)}{3}-\omega-\alpha}^{\frac{3\cdot(2\pi)}{3}-\omega-2\alpha}\frac{d\varphi}{2\pi}\frac{\frac{2\pi}{3}-\alpha}{2\pi}\right) = \frac{(2\pi-3\alpha)^3}{36\pi^3}. \tag{A2}$$

Thus, the probability for a disk with $n=3$ EQ-type patches covering no edge ($z=0$) is

$$p(n=3,z=0) = \frac{Z(n=3,z=0)}{Z(n=3)} = \frac{2\pi-3\alpha}{9\pi}. \tag{A3}$$

For RSA-type patches, n patches are sequentially placed on a disk. The patches placed later will be affected by those placed earlier. For the first patch, a random number in $[0, 2\pi)$ is used, and for later patches, the ranges of random numbers are gradually reduced. The probability of successfully placing three nonoverlapping patches on a disk is

$$\frac{Z(n=3)}{Z} = \frac{2\pi}{2\pi}\left(\int_0^{2\pi-3\alpha}\frac{d\varphi}{2\pi-2\alpha}\frac{2\pi-3\alpha-\varphi}{2\pi-3\alpha-\varphi} + \int_\alpha^{2\pi-2\alpha}\frac{d\varphi}{2\pi-2\alpha}\frac{\varphi-\alpha}{\varphi-\alpha}\right) = \frac{2\pi-3\alpha}{\pi-\alpha}. \tag{A4}$$

The probability that there are three patches occupying no edge is

$$\frac{Z(n=3,z=0)}{Z} = 3\int_0^{\frac{2\pi}{3}-\alpha}\frac{d\omega}{2\pi}\left(\int_{\frac{2\pi}{3}-\omega-\alpha}^{\frac{2\cdot(2\pi)}{3}-\omega-2\alpha}\frac{d\varphi}{2\pi-2\alpha}\frac{\frac{2\pi}{3}-\alpha}{2\pi-3\alpha-\varphi} + \int_{\frac{2\cdot(2\pi)}{3}-\omega-\alpha}^{\frac{3\cdot(2\pi)}{3}-\omega-2\alpha}\frac{d\varphi}{2\pi-2\alpha}\frac{\frac{2\pi}{3}-\alpha}{\varphi-\alpha}\right) = \frac{(2\pi-3\alpha)^2\left(\ln 3-\frac{4}{3}\ln 2\right)}{2\pi(\pi-\alpha)}. \tag{A5}$$

Therefore, the probability for a disk with $n=3$ RSA-type patches covering no edge ($z=0$) is

$$p(n=3,z=0) = \frac{Z(n=3,z=0)}{Z(n=3)} = \frac{(2\pi-3\alpha)\left(\ln 3-\frac{4}{3}\ln 2\right)}{2\pi}. \tag{A6}$$

Comparing the above Eq. (A3) and Eq. (A6), one sees that patches of the EQ type and RSA type lead to different probabilities, $p(n=3,z=0)$. Generally, for $n\geqslant 3$ and $z\geqslant 0$, in similar ways one can verify that the two types of random patches lead to different occupation probabilities $p(n,z)$.

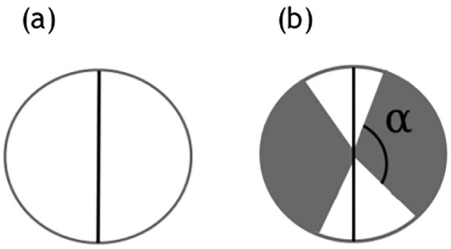

FIG. 11. (a) Two edges divide a disk into two regions of equal area. (b) A configuration in which two patches are randomly placed on a disk and they occupy no edge.

APPENDIX B: OCCUPATION OF TWO EDGES BY TWO NONOVERLAPPING RANDOM PATCHES

Below we show that, for $n=2$, the two types of random patches lead to the same $p(n=2,z=0)$. In Fig. 11(a) two edges divide a disk into two regions of equal area. Assuming that the size of a patch satisfies $\alpha = 2\theta < \pi$ and $2\alpha = 4\theta > \pi$, a patch can occupy at most one edge, and a region can contain at most one patch since patches cannot overlap, as in Fig. 11(b).

For patches of the EQ type, two random numbers in $[0, 2\pi)$ are used to give positions the two patches. The probability that the two patches do not overlap is

$$\frac{Z(n=2)}{Z} = \frac{2\pi-2\alpha}{2\pi} = \frac{\pi-\alpha}{\pi}, \tag{B1}$$

and the probability that two patches do not overlap and do not occupy any edge is

$$\frac{Z(n=2,z=0)}{Z} = \frac{2(\pi-\alpha)}{2\pi}\cdot\frac{\pi-\alpha}{2\pi} = \frac{(\pi-\alpha)^2}{2\pi^2}. \tag{B2}$$

Thus the probability for a disk with $n=2$ EQ-type patches covering no edge ($z=0$) is

$$p(n=2,z=0) = \frac{Z(n=2,z=0)}{Z(n=2)} = \frac{\pi-\alpha}{2\pi}. \tag{B3}$$

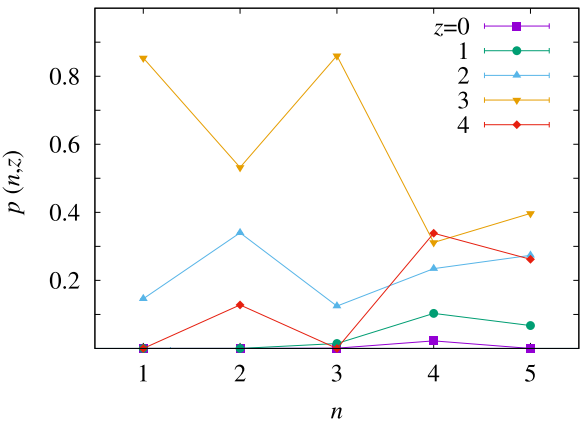

FIG. 12. Probability $p(n,z)$ for a particle with n RSA-type patches covering z neighboring edges on the square lattice at $\chi_c(n)$. At fixed n, one has $\sum_{z=0}^{4} p(n,z) = 1$. Error bars are smaller than the data points.

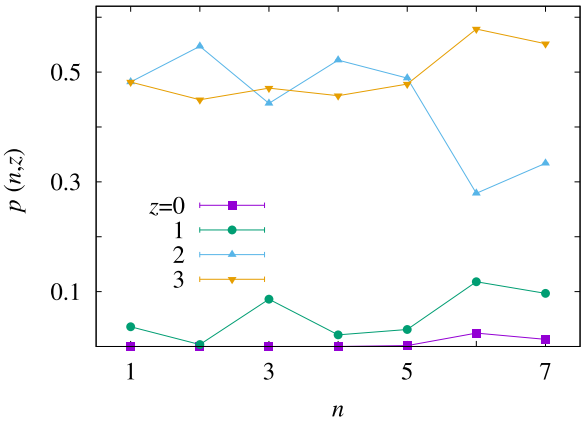

FIG. 13. Probability $p(n, z)$ for a particle with n RSA-type patches covering z neighboring edges on the honeycomb lattice at $\chi_c(n)$. At fixed n, one has $\sum_{z=0}^{3} p(n, z) = 1$. Error bars are smaller than the data points.

For patches of the RSA type, two patches can always be successfully placed on a disk, i.e.,

$$\frac{Z(n=2)}{Z} = 1, \tag{B4}$$

and the probability that the two patches do not occupy any edge is

$$\frac{Z(n=2, z=0)}{Z} = \frac{2(\pi-\alpha)}{2\pi}\frac{\pi-\alpha}{2\pi-2\alpha} = \frac{\pi-\alpha}{2\pi}. \tag{B5}$$

Therefore, the probability for a disk with $n = 2$ RSA-type patches covering no edge ($z = 0$) is

$$p(n=2, z=0) = \frac{Z(n=2, z=0)}{Z(n=2)} = \frac{\pi-\alpha}{2\pi}. \tag{B6}$$

Comparing Eqs. (B3) and (B6), one sees that patches of the EQ type and RSA type lead to the same probability $p(n = 2, z = 0)$. At other z values, similarly one can also prove that the two types of random patches lead to same values of $p(n = 2, z)$.

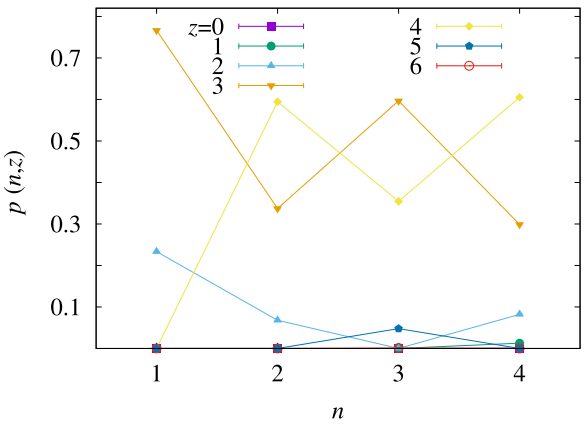

FIG. 14. Probability $p(n, z)$ for a particle with n RSA-type patches covering z neighboring edges on the triangular lattice at $\chi_c(n)$. At fixed n, one has $\sum_{z=0}^{6} p(n, z) = 1$. Error bars are smaller than the data points.

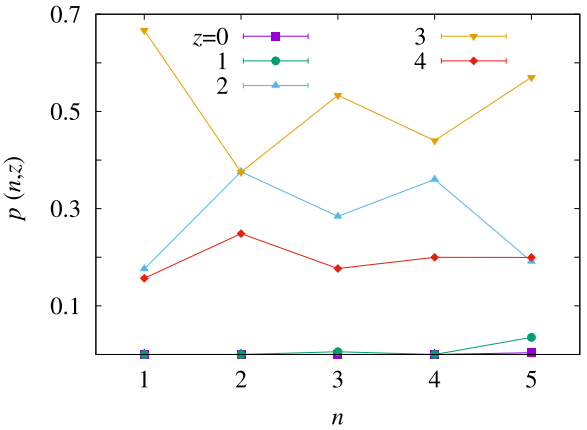

FIG. 15. Probability $p(n, z)$ of a particle with n RSA-type patches covering z neighboring edges on the kagome lattice at $\chi_c(n)$. At fixed n, one has $\sum_{z=0}^{4} p(n, z) = 1$. Error bars are smaller than the data points.

APPENDIX C: PLOT OF $p(n, z)$ ON FOUR LATTICES

The plots of $p(n, z)$ are shown in Figs. 12, 13, 14, and 15, for the square, honeycomb, triangular, and kagome lattices, respectively. These plots help understand the non-monotonic change of $\chi_c(n)$, as explained in the main text.

APPENDIX D: SAME χ_c VALUE FOR $n \leqslant 2$ ON THE HONEYCOMB LATTICE

For $n = 1$, since there is no distinction between three types (SYM type, EQ type, and RSA type) of patches, there is only a single value of $\chi_c(1)$ on a given lattice. For $n = 2$, one has $\chi_c^{\mathrm{EQ}}(2) = \chi_c^{\mathrm{RSA}}(2)$ since the EQ-type and RSA-type patches share the same $p(n = 2, z)$, as shown in Appendix B. On the honeycomb lattice, considering the above and $\chi_c^{\mathrm{SYM}}(2) = \chi_c(1)$ from Ref. [12], if $\chi_c^{\mathrm{EQ}}(2) = \chi_c(1)$, one could conclude that the three types of patches lead to the same χ_c value for $n \leqslant 2$. We demonstrate below that $\chi_c^{\mathrm{EQ}}(2) = \chi_c(1)$ indeed holds.

On the honeycomb lattice, for $n = 1$, in Ref. [12] near χ_c, it is found that $p(z = 2) = 3(1 - \chi)$, $p(z = 3) = 3\chi - 2$, and $p(z = 2) + p(z = 3) = 1$. Figure 16 is a snapshot for a particle with $n = 2$ EQ-type patches on the honeycomb lattice. It can be derived that near $\chi_c = 0.812\,301(4)$ (from Table IV) one has $p(z = 3) = 6\int_0^{\chi/2-1/3} d\sigma = 3\chi - 2$ and $p(z = 2) = 3(1 - \chi)$. These values are the same as those for $n = 1$, which leads to $\chi_c^{\mathrm{EQ}}(2) = \chi_c(1)$.

FIG. 16. Snapshot of a particle with two random patches on the honeycomb lattice. The patches occupy three edges when the patch at the left top is rotated counterclockwise by a small angle, and they cover two edges when the patch is rotated clockwise by a small angle.

[1] P. J. Flory, Molecular size distribution in three dimensional polymers. I. Gelation, J. Am. Chem. Soc. **63**, 3083 (1941).

[2] S. R. Broadbent and J. M. Hammersley, Percolation processes I. Crystals and mazes, Math. Proc. Camb. Phil. Soc. **53**, 629 (1957).

[3] D. Stauffer and A. Aharony, *Introduction to Percolation Theory*, 2nd ed. (Taylor & Francis, London, 1992).

[4] A. A. Saberi, Recent advances in percolation theory and its applications, Phys. Rep. **578**, 1 (2015).

[5] M. Sheinman, A. Sharma, J. Alvarado, G. H. Koenderink, and F. C. MacKintosh, Anomalous discontinuity at the percolation critical point of active gels, Phys. Rev. Lett. **114**, 098104 (2015).

[6] H. Hu, R. M. Ziff, and Y. J. Deng, No-enclave percolation corresponds to holes in the cluster backbone, Phys. Rev. Lett. **117**, 185701 (2016).

[7] F. Sciortino, E. Zaccarelli, Equilibrium gels of limited valence colloids, Curr. Opin. Colloid Interface Sci. **30**, 90 (2017).

[8] J. F. Fan, J. Meng, J. Ludescher, X. S. Chen, Y. Ashkenazy, J. Kurths, S. Havlin, and H. J. Schellnhuber, Statistical physics approaches to the complex Earth system, Phys. Rep. **896**, 1 (2021).

[9] R. M. Ziff, Percolation and the pandemic, Physica A **568**, 125723 (2021).

[10] H. Hu, R. M. Ziff, and Y. J. Deng, Universal critical behavior of percolation in orientationally ordered Janus particles and other anisotropic systems, Phys. Rev. Lett. **129**, 278002 (2022).

[11] Y. Ma, M. Hanks, and M. S. Kim, Non-Pauli errors can be efficiently sampled in qudit surface codes, Phys. Rev. Lett. **131**, 200602 (2023).

[12] Q. C. Wang, Z. F. He, J. F. Wang, and H. Hu, Percolation thresholds of randomly rotating patchy particles on Archimedean lattices, Phys. Rev. E **105**, 034118 (2022).

[13] J. Lahann, Recent progress in nano-biotechnology: Compartmentalized micro- and nanoparticles via electrohydrodynamic co-jetting, Small **7**, 1149 (2011).

[14] A. Walther and A. H. E. Müller, Janus particles: synthesis, self-assembly, physical properties, and applications, Chem. Rev. **113**, 5194 (2013).

[15] J. Zhang, B. A. Grzybowski, and S. Granick, Janus particle synthesis, assembly, and application, Langmuir **33**, 6964 (2017).

[16] J. W. Evans, Random and cooperative sequential adsorption, Rev. Mod. Phys. **65**, 1281 (1993).

[17] C. R. Scullard and R. M. Ziff, Critical surfaces for general bond percolation problems, Phys. Rev. Lett. **100**, 185701 (2008).

[18] C. R. Scullard and R. M. Ziff, Critical surfaces for general inhomogeneous bond percolation problems, J. Stat. Mech. (2010) P03021.

[19] C. R. Scullard, Polynomial sequences for bond percolation critical thresholds, J. Stat. Mech. (2011) P09022.

[20] C. R. Scullard, Percolation critical polynomials as a graph invariant, Phys. Rev. E **86**, 041131 (2012).

[21] C. R. Scullard and J. L. Jacobsen, Transfer matrix computation of generalized critical polynomials in percolation, J. Phys. A: Math. Theor. **45**, 494004 (2012).

[22] J. L. Jacobsen, High-precision percolation thresholds and Potts-model critical manifolds from graph polynomials, J. Phys. A: Math. Theor. **47**, 135001 (2014).

[23] J. L. Jacobsen, Critical points of Potts and O(N) models from eigenvalue identities in periodic Temperley-Lieb algebras, J. Phys. A: Math. Theor. **48**, 454003 (2015).

[24] C. R. Scullard and J. L. Jacobsen, Potts-model critical manifolds revisited, J. Phys. A: Math. Theor. **49**, 125003 (2016).

[25] C. R. Scullard and J. L. Jacobsen, Bond percolation thresholds on Archimedean lattices from critical polynomial roots, Phys. Rev. Res. **2**, 012050(R) (2020).

[26] W. H. Xu, J. F. Wang, H. Hu, and Y. J. Deng, Critical polynomials in the nonplanar and continuum percolation models, Phys. Rev. E **103**, 022127 (2021).

[27] X. X. Zhang and H. Hu, Phase behavior and percolation in an equilibrium system of symmetrically interacting Janus disks on the triangular lattice, Chin. Phys. B **32**, 080502 (2023).

[28] M. J. Kartha and A. G. Banpurkar, Why patchy diffusion-limited aggregation belongs to the directed-percolation universality class, Phys. Rev. E **94**, 062108 (2016).

[29] J. L. B. de Araújo, F. F. Munarin, G. A. Farias, F. M. Peeters, and W. P. Ferreira, Structure and reentrant percolation in an inverse patchy colloidal system, Phys. Rev. E **95**, 062606 (2017).

[30] G. Wang and J. W. Swan, Surface heterogeneity affects percolation and gelation of colloids: Dynamic simulations with random patchy spheres, Soft Matter **15**, 5094 (2019).

[31] J. Song, M. H. Rizvi, B. B. Lynch, J. Ilavsky, D. Mankus, J. B. Tracy, G. H. McKinley, and N. Holten-Andersen, Programmable anisotropy and percolation in supramolecular patchy particle gels, ACS Nano **14**, 17018 (2020).

[32] F. Seiferling, D. de las Heras, and M. M. Telo da Gama, Percolation in binary and ternary mixtures of patchy colloids, J. Chem. Phys. **145**, 074903 (2016).

[33] R. P. Langlands, C. Pichet, Ph. Pouliot, and Y. Saint-Aubin, On the universality of crossing probabilities in two-dimensional percolation, J. Stat. Phys. **67**, 553 (1992).

[34] H. T. Pinson, Critical percolation on the torus, J. Stat. Phys. **75**, 1167 (1994).

[35] S. C. Kapfer and W. Krauth, Irreversible local Markov chains with rapid convergence towards equilibrium, Phys. Rev. Lett. **119**, 240603 (2017).

[36] V. I. Manousiouthakis and M. W. Deem, Strict detailed balance is unnecessary in Monte Carlo simulation, J. Chem. Phys. **110**, 2753 (1999).

[37] G. Zhang and S. Torquato, Precise algorithm to generate random sequential addition of hard hyperspheres at saturation, Phys. Rev. E **88**, 053312 (2013).

[38] Z. W. Salsburg, R. W. Zwanzig, and J. G. Kirkwood, Molecular distribution functions in a one-dimensional fluid, J. Chem. Phys. **21**, 1098 (1953).

[39] R. L. Sells, C. W. Harris, and E. Guth, The pair distribution function for a one-dimensional gas, J. Chem. Phys. **21**, 1422 (1953)

[40] M. F. Sykes and J. W. Essam, Exact critical percolation probabilities for site and bond problems in two dimensions, J. Math. Phys. **5**, 1117 (1964).

[41] X. B. Wang, W. L. Liu, J. Wang, and H. Hu (unpublished).

[42] T. Tomé and R. M. Ziff, Critical behavior of the susceptible-infected-recovered model on a square lattice, Phys. Rev. E **82**, 051921 (2010).

[43] A. P. Furlan, D. C. dos Santos, R. M. Ziff, and R. Dickman, Jamming and percolation of dimers in restricted-valence random sequential adsorption, Phys. Rev. Res. **2**, 043027 (2020).